J Mater Sci (2011) 46:2242–2250
DOI 10.1007/s10853-010-5063-6

Evolution of microstructure induced by calcination in leached Al–Cu–Fe quasicrystal and its effects on catalytic activity

Toyokazu Tanabe · Satoshi Kameoka · An Pang Tsai

Received: 27 July 2010 / Accepted: 9 November 2010 / Published online: 30 November 2010

Abstract Effects of calcination on catalytic activity for steam reforming of methanol (SRM) over an Al–Cu–Fe quasicrystal (QC) leached with NaOH aq. have been investigated in terms of microstructure with X-ray diffraction and transmission electron microscope (TEM). Calcination at 600 °C in air drastically improved the catalytic activity of the leached QC. TEM observations on cross-section of the samples revealed that cubic $Cu_xFe_{3-x-y}Al_yO_4$ spinel was formed at the outermost layer of the leached QC after calcinations. Prior to the catalytic reaction, the $Cu_xFe_{3-x-y}Al_yO_4$ spinel decomposed to a composite where fine Cu nanoparticles dispersed in $(Fe,Al)_3O_4$ matrix under H_2 treatment at 300 °C. Drastic increase in catalytic activity is responsible for the fine Cu nanoparticles in the composite. The Cu nanoparticles sit along the same orientation with $(Fe,Al)_3O_4$, e.g., Cu [013]// $(Fe,Al)_3O_4$ [013] and Cu [200]//$(Fe,Al)_3O_4$ [400]. This orientation relationship may stabilize the Cu nanoparticles through a bonding of Cu–O–Fe.

T. Tanabe (✉)
Institute for Materials Research (IMR), Tohoku University, 2-1-1 Katahira, Aoba-ku, Sendai 980-8577, Japan
e-mail: tanabe@tagen.tohoku.ac.jp

T. Tanabe · S. Kameoka · A. P. Tsai
Institute of Multidisciplinary Research for Advanced Materials (IMRAM), Tohoku University, 2-1-1 Katahira, Aoba-ku, Sendai 980-8577, Japan

A. P. Tsai
National Institute of Materials Science (NIMS), Tsukuba 305-0047, Japan

Introduction

Quasicrystals (QCs) were discovered in 1984 by Shechtman et al. [1] and are typically binary, ternary, or quaternary intermetallic compounds. They have well-ordered structure without periodicity, and posses rotational symmetries forbidden in crystallography (i.e., 5-fold and 10-fold symmetries). These extraordinary materials not only have unique structure, but also have unusual properties such as high electrical resistance, high hardness, and low friction coefficient [2]. They cannot be applied as structural materials owing to their brittle nature at ambient temperature. While, high surface area is generally required for a catalyst and the brittleness of QCs allows them to crush to obtain fine particles with high surface areas. Moreover, many QCs have a good composition which includes a catalytic active element, such as Pd, Ni, or Cu. Therefore, they have potential to be catalyst.

Some studies of the application of QC for catalysis have been reported. Thin film of Al–Cu–Fe QC were applied for synthesis of carbon nanotubes [3] and Ti-based QC powder showed high activity and selectivity for the oxidation of cyclohexane [4]. Tsai and Yoshimura [5, 6] first employed leaching treatment with alkali solution in the preparation of catalysts from Al–Cu–Fe QC alloys. Recently, several Al-based QCs (Al–Cu–Fe [7–9], Al–Cu–Ru [10], Al–Ni–Co [11]) have been applied to catalyst by employing an alkali-leaching treatment. This Al leaching process with alkali solution is the same as that which by the one is applied to Raney catalysts which are made from Al-based alloys [12]. It has been reported that NaOH-leached Al–Cu–Fe QCs showed excellent activity for the steam reforming of methanol (SRM: $CH_3OH + H_2O \rightarrow 3H_2 + CO_2$) [7]. A leached region composed of active metal nanoparticles is created by selectively dissolving Al from Al-based QC

alloys by means of leaching. Although the leached region dominates the catalytic activity and stability of leached QC catalysts, it is difficult to observe the leached region with TEM owing to narrow electron transparency area. Thus, for a long time the origin of high activity for leached alloys including Raney catalysts remained unclear. Sample preparation for TEM observation has been a key factor to understand high activity responsible for microstructure for catalysts synthesized by leaching. Smith et al. [13] have observed the porous Cu of a Raney Cu catalyst using a focused ion beam (FIB) miller and a TEM. Nevertheless, this method cannot avoid the damage induced by focused Ga ion beam irradiation. Recently [14, 15], we have succeeded in observing cross-sectional microstructure of leached regions with 100-nm thick on a catalyst particle using a resin-embedded sample and Ar ion milling method. This has opened the door to understand the origin of catalytic activity in terms of metallurgical microstructures.

More recently, we further found significant enhancement of catalytic activity arose from calcinations in a leached Al–Cu–Fe QC alloy. This phenomenon is in contrast to that observed in typical catalysts where sintering induced by calcinations and consequently a serious deactivation occurred. If the contribution of microstructure change induced by calcination on catalytic properties was clear, we would be able to employ the same principle to design new alloy catalysts intentionally. In this article, we study the modification of the microstructure induced by calcinations (and/or reduction) by means of TEM observation on cross-sectional leached Al–Cu–Fe QC alloy particles. We discuss the contribution of change in microstructure on catalytic activity and suggest a plausible model to understand their relationship.

Experimental

Precursor QC alloy preparation

Al–Cu–Fe QC ($Al_{63}Cu_{25}Fe_{12}$ at%) alloy ingots were prepared by melting mixtures of pure elements with purities of 99.9 wt% Al, 99.9 wt% Cu, and 99.9 wt% Fe in an argon atmosphere using an arc furnace. An annealing treatment for 24 h at 800 °C under vacuum was applied to the as-cast ingots. Subsequently, powdered alloys were obtained by crushing and screening the annealed ingots to a particle size of 20–53 μm.

Catalyst preparation

Leached Al–Cu–Fe QC alloys were prepared by alkali leaching of the precursor alloys (2 g), which were leached in a 5 wt% NaOH aqueous solution (120 mL) for 4 h at room temperature to remove the Al (OH/Al = 3.1). The concentration of dissolved metal ions in the leaching solution was analyzed by ICP spectrophotometer (Perkin-Elmer, Optima 3300). Upon the leaching, ca. 60% Al in the precursor QC alloy dissolves into the leaching solution. No any Cu and Fe were detected by ICP analysis. The NaOH-leached powders were filtered out and thoroughly washed with distilled water until no alkali was detected in the filtrate and dried at 50 °C overnight. Finally, the resultant powders were calcined at 600 °C for 3 h in air.

For comparison, $CuFeAlO_4$ and CuO were also studied. $CuFeAlO_4$ spinel was synthesized from stoichiometric oxide mixture of CuO, Al_2O_3 (>99.5% purities; NanoTek, Kanto Chemical Co.), and α-Fe_2O_3 (> 99.5% purity; NanoTek, C.I. Kasei Co.). The mixture were calcined in air at 1,100 °C for 12 h. CuO was precalcinated in air at 600 °C for 3 h. In addition, a Cu/ZnO catalyst (Cu:Zn = 3:7 mol ratio) was prepared by a conventional coprecipitation method. A mixed aqueous solution of copper and zinc nitrate (1.0 mol/L) and an aqueous solution of sodium carbonate (1.0 mol/L) were simultaneously added dropwise to distilled water while being stirred. The formed precipitates were then aged at room temperature for 48 h, and were then filtered, washed with distilled water, dried at 120 °C overnight, and calcined at 350 °C for 3 h in air.

Sample characterization

The bulk structures of each sample were identified by means of X-ray diffraction (XRD). High resolution XRD measurements were carried out using the high brilliant synchrotron radiation in BL15XU ($\lambda = 0.65297$ Å) of SPring-8 at the Japan Synchrotron Radiation Research Institute. Normal XRD measurements were performed using Cu K_α ($\lambda = 1.543$ Å) operating at 40 kV and 30 mA (Rigaku, RINT 2500). Using a surface area analyzer (BEL Japan, Belsorp-mini), specific BET surface areas of the catalyst particles were determined by their N_2 adsorption at −196 °C. Temperature-programmed reduction (TPR) was carried out using 50 mg of catalyst from room temperature to 400 °C at a heating rate of 4 °C/min in 5% H_2/Ar flow (30 mL/min). N_2O titration measurements were carried out with a conventional pulse titration method [16]. The N_2O titrations were calculated from the total amount of N_2O consumption at 90 °C. Prior to the N_2O chemisorptions, each catalyst was reduced in 5% H_2/Ar for 1 h at 250 °C in a conventional flow reactor.

Steam reforming of methanol reaction

SRM reactions ($CH_3OH + H_2O \rightarrow 3H_2 + CO_2$) were carried out in a conventional flow reactor at atmospheric

pressure. All the catalysts were pretreated in the flow reactor with 50% H_2/N_2 at 300 °C for 20 min. The standard reaction conditions were 32% of methanol, 48% of H_2O, and N_2 (balance) at a liquid hourly space velocity of 60–70 h^{-1} (GHSV = 76,000, $CH_3OH/H_2O = 2/3$) with a catalyst bed weight of 0.2 g (density = 1.3 g/cm^3). The gas products after water trapping were monitored by an on-line gas chromatograph (TCD) (Shimadzu, GC-14B). The catalytic activities of the SRM were evaluated by the H_2 production rates per BET surface area (μmol/s/m^2_{cat}), and per N_2O titration (μmol/s/μmol (N_2O)).

Cross-sectional observation with TEM

TEM specimens for cross-sectional observation were prepared by a method that employed resin-embedding and Ar ion milling. The catalyst powders were mixed with resins (Koyo chemicals, KPR-30) and dropped onto a Mo mesh. After thermosetting at 80 °C for 4 h, the resins were thinned with a focused Ar ion miller (JEOL, EM-09100IS). TEM analysis was carried out with a JEOL 2010 microscope with an operating voltage of 200 kV. The composition of the catalyst powders was analyzed by an EDS spectrometer, which is an Oxford link system that which was attached onto the TEM.

Results and discussion

Effect of calcination on catalytic activity for SRM reaction

Figure 1a shows catalytic activity expressed with H_2 production rates per surface area as a function of reaction temperatures for SRM reaction ($CH_3OH + H_2O \rightarrow 3H_2 + CO_2$) over NaOH-leached Al–Cu–Fe QC alloys with and without calcination at 600 °C. Cu catalyst is known as one of promising catalysts for this reaction. The product gas contained H_2 and CO_2 as the major components for SRM reaction catalyzed by two samples shown in Fig. 1a, indicating that these two samples are basically Cu catalysts but have different distribution and particle size of Cu which are account for difference in activity. The H_2 production rates of the leached QC alloys were increased by about five times over all reaction temperatures after calcination at 600 °C. Figure 1b shows methanol conversions as a function of time on-stream at 320 °C. The stability of the leached QC after calcination was comparable to that of the Cu/ZnO catalyst. These imply that calcinations promoted generation of large number of effective Cu species (i.e., fine Cu nanoparticle) exposed to reaction. The enhancement induced by calcinations is not observed in conventional Cu based mixed catalysts (e.g., Cu/ZnO/Al_2O_3) whose catalytic activities gradually decreased with an increase in calcination temperatures [17, 18].

Calcination behavior of leached QC

Figure 2 shows powder XRD patterns for precursor QC alloy and NaOH-leached QC alloy with and without calcination at 600 °C. The precursor alloy consists of a mostly quasicrystalline (QC) phase [19]. Before calcination (as leached), the peaks of Cu and Cu_2O were observed in the diffraction patterns. After calcination, those of CuO were appeared mainly and there were many weak peaks which cannot be assigned in the normal XRD measurements.

In our previous papers [14, 15], we have directly observed cross-sectional microstructure of NaOH-leached Al–Cu–Fe QC alloy before calcination by a TEM as shown in Fig. 3, and confirmed that a leached layer composed of homogeneous mixture of oxides containing Cu, Fe, Al, which was formed at the outer layer of the particle and precursor QC phase persisted in the core area. The leached layer/unleached QC ratio was around 55% assumed by TEM images. With this in mind, Fig. 4 shows the cross-sectional microstructure of NaOH-leached Al–Cu–Fe QC

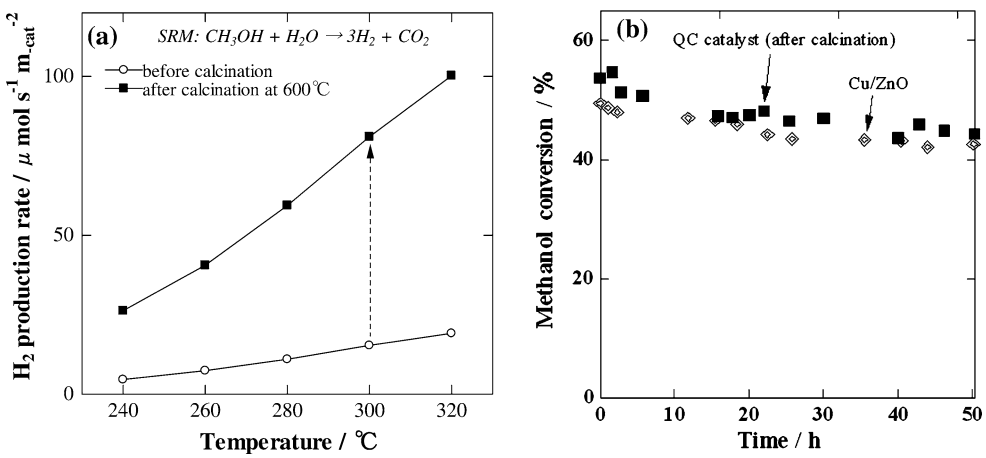

Fig. 1 **a** H_2 production rates per surface area as a function of reaction temperatures for SRM reaction of NaOH-leached Al–Cu–Fe QC alloys with and without calcination at 600 °C and **b** methanol conversions as a function of time on-stream at 320 °C over leached Al–Cu–Fe QC with calcination and Cu/ZnO catalyst

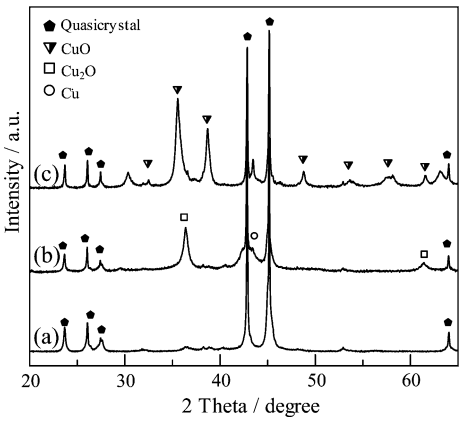

Fig. 2 Powder X-ray diffraction patterns for (*a*) precursor QC alloy, (*b*) NaOH-leached Al–Cu–Fe QC alloy (before calcination), and (*c*) after calcination at 600 °C

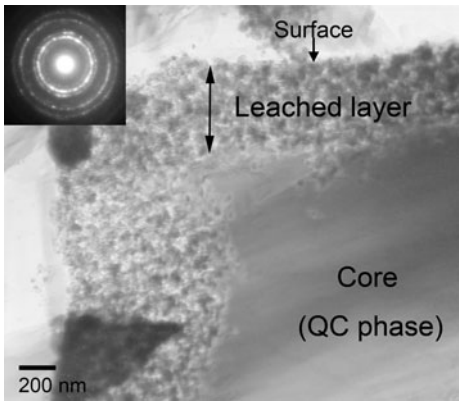

Fig. 3 Bright field image of cross-section of NaOH-leached Al–Cu–Fe QC alloy before calcination (*inset* electron diffraction pattern obtained from the leached layer)

alloy after further calcination at 600 °C (hereafter *calcined QC*). Figure 4a shows bright field image where the homogeneous leached layer with uniform thickness of about 500 nm was maintained in the particles. The selected area electron diffraction (SAD) pattern (Fig. 4a, inset) obtained from the core of particle has verified the presence of the QC phase in the particles even after the calcination. It was also observed that the formation of cubic β phase (i.e., B2 phase of Al(Fe,Cu)) at local region in the core (not shown). Figure 4b shows bright field image around the leached layer of the *calcined QC*. Figure 4d is a SAD pattern taken from the surface of the leached layer of Fig. 4b. The SAD corresponds to [111] incidence of FCC lattice ($a = 8.3$ Å) which has a similar structure of Fe_3O_4 spinel with space group of $Fd\bar{3}m$ ($a = 8.396$ Å). Figure 4c is a dark-field image excited by the 2–20 reflection of Fig. 4d. The bright contrast in the image corresponds to the spinel structure with 50-nm thick on the surface of the particle. The cross-sectional observation verified the formation of the spinel structure on the surface of the *calcined QC*. Figure 5 shows XRD pattern using high brilliant synchrotron radiation for the *calcined QC*, where reference data of Fe_3O_4 (PDF#19-0627) are also shown for comparison. Using synchrotron radiation, a number of weak peaks were clearly observed and can be assigned owing to high intensity compared to conventional XRD (Fig. 2). The peaks consisted of CuO, β phase, QC phase (precursor), and spinel phase with similar structure to Fe_3O_4. The high resolution XRD result reconfirmed the formation of the spinel phase isostructural to Fe_3O_4 in the *calcined QC*. It was found that the diffraction peaks of the spinel phase were at a higher reciprocal Q vectors compared with those of Fe_3O_4 as shown in the inset of Fig. 5. The Fe_3O_4 has an inverse-spinel structure in which the tetragonal site is occupied by Fe^{3+} and the octahedral site by an equal share of Fe^{2+} and Fe^{3+} (see Fig. 6). Composition analysis with EDS (Fig. 4e) showed the presence of Cu and Al in addition to Fe and O in the spinel phase on the *calcined QC*. Fe^{2+} and Fe^{3+} of Fe_3O_4 can be partially or completely substituted by Cu^{2+} and Al^{3+}, respectively, without changing spinel structure. The substitution by Cu^{2+} and Al^{3+} arises a decrease in lattice constant in the spinel structure [20, 21], because effective ionic radii of octahedral Cu^{2+} (0.73 Å), Al^{3+} (0.53 Å), and tetrahedral Al^{3+} (0.39 Å) are smaller than those of octahedral Fe^{2+} (0.77 Å), Fe^{3+} (0.65 Å), and tetrahedral Fe^{3+} (0.49 Å), respectively [22]. The lattice constant of the spinel phase on the *calcined QC* estimated from the XRD result (Fig. 5) is shown together with those of cubic spinel phases in Cu–Fe–Al–O system in Table 1. The lattice constant of the spinel phase on the *calcined QC* is quite close to that of $Cu_{0.95}Fe_{1.05}AlO_4$ [23]. The XRD and TEM results confirmed the formation of $Cu_xFe_{3-x-y}Al_yO_4$ on the *calcined QC*. Shimoda et al. [24] have also reported that cubic $Cu_xFe_{3-x-y}Al_yO_4$ spinel was formed by heat treatment of pre-reduced $CuFe_2O_4$–Al_2O_3 composites in air at 500–700 °C, in consistent with our results. Considering the content of Cu in the leached layer of leached QC alloy, it is reasonable that a part of Cu is incorporated in $Cu_xFe_{3-x-y}Al_yO_4$ spinel and the rest forms CuO upon calcinations as shown in Figs. 4 and 5.

Reduction behavior of calcined QC

Figure 7 shows H_2-TPR (temperature-programmed reduction) profile from room temperature to 400 °C for the *calcined QC*. The profile of the *calcined QC* consisted of a major peak appearing at temperature around 200 °C. It was reported that the reduction peaks of CuO and $Cu_xFe_{3-x-y}Al_yO_4$ also appeared around 200–300 °C [24, 25]. These results indicate that the reduction peak of the *calcined QC* was ascribed to the reduction of two components, i.e., the

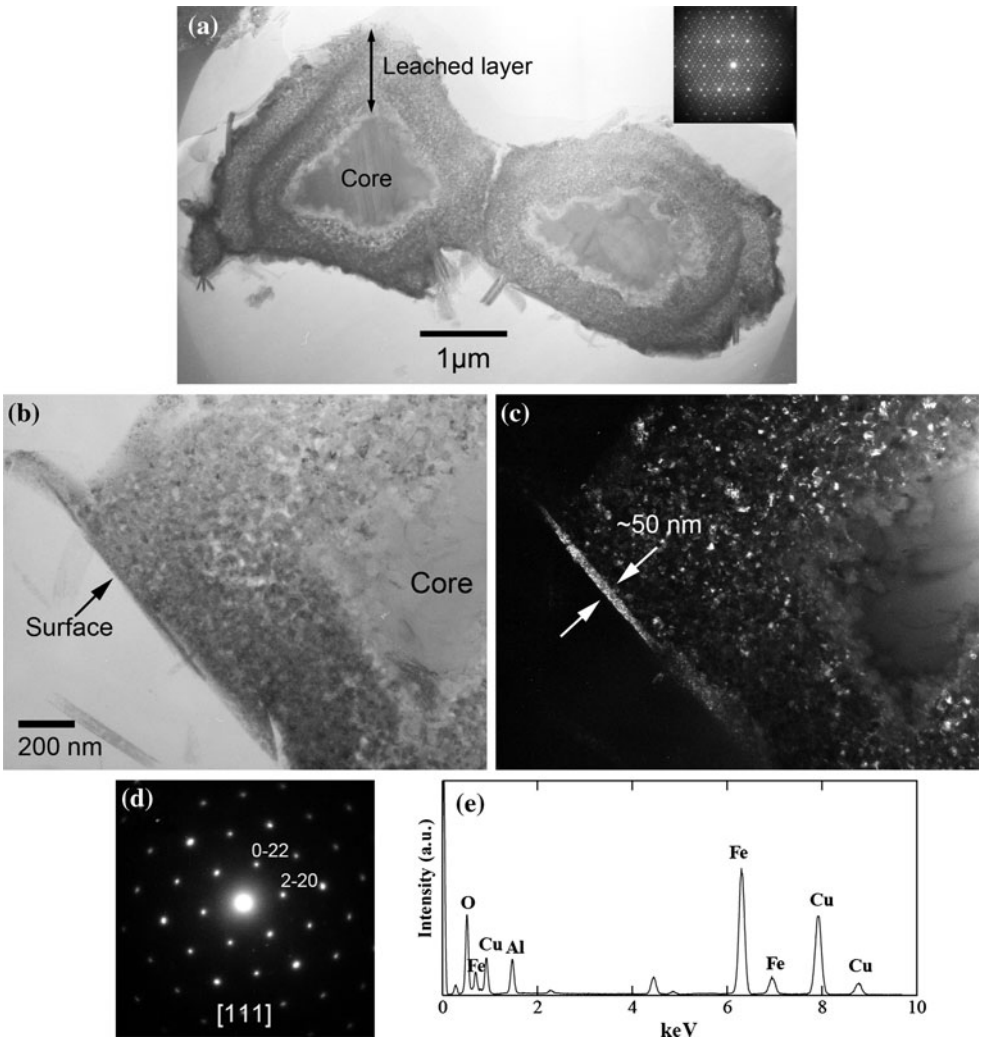

Fig. 4 **a** Bright field image of cross-section of NaOH-leached Al–Cu–Fe QC alloy after calcination at 600 °C, **b** bright field image around the leached layer, **c** dark-field image using 2–20 reflection of cubic spinel, **d** selected area diffraction (SAD) pattern, and **e** EDS spectrum obtained from the spinel in (**b**)

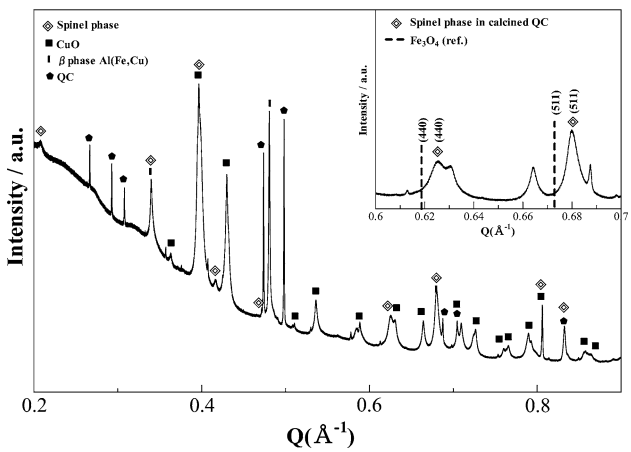

Fig. 5 Powder XRD pattern using high brilliant synchrotron radiation for NaOH-leached Al–Cu–Fe QC alloy after calcination at 600 °C. Reference data of Fe_3O_4 (PDF #19-0627) are also shown for comparison

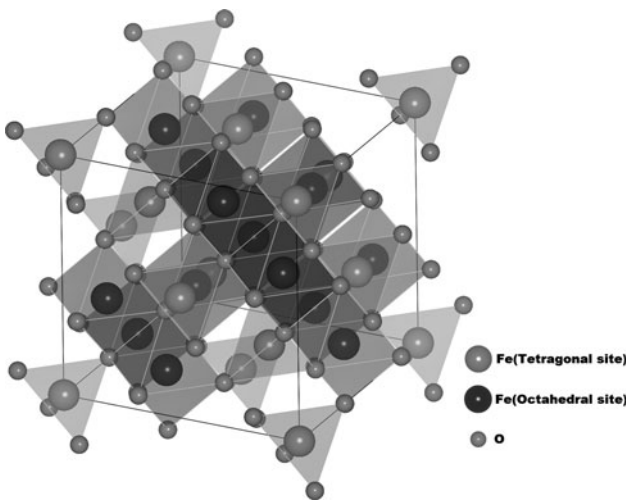

Fig. 6 Crystal structure for Fe_3O_4

reduction of CuO and $Cu_xFe_{3-x-y}Al_yO_4$. Figure 8 shows the powder XRD patterns for the *calcined QC* after H_2 reduction at 300 °C. Those of CuO and $CuFeAlO_4$ powders after reduction are also shown for comparison. Upon the reduction of the *calcined QC*, metallic Cu and $(Fe,Al)_3O_4$ were observed. $CuFeAlO_4$ powder was also reduced to

Table 1 Lattice constant of cubic spinel phases in Cu–Fe–Al–O system

Cubic spinel phase	a (Å)	Space group	Reference
Fe_3O_4 (magnetite)	8.3970	$Fd\bar{3}m$	[31]
$CuFe_2O_4$ (coprospinel)	8.369	$Fd\bar{3}m$	[32]
Spinel @ calcined QC	8.32	–	This study
$Cu_{0.95}Fe_{1.05}AlO_4$	8.3235	$Fd\bar{3}m$	[23]
$FeAl_2O_4$ (hercynite)	8.15579	$Fd\bar{3}m$	[33]

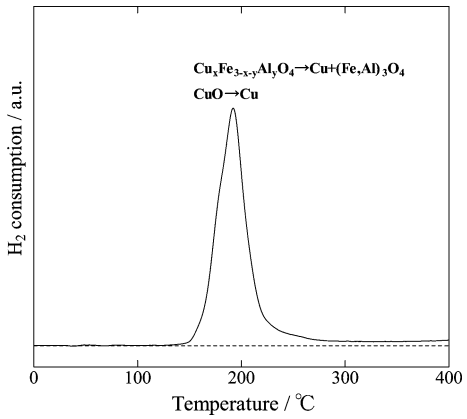

Fig. 7 H_2-TPR (temperature-programmed reduction) profile for NaOH-leached Al–Cu–Fe QC alloy after calcination at 600 °C

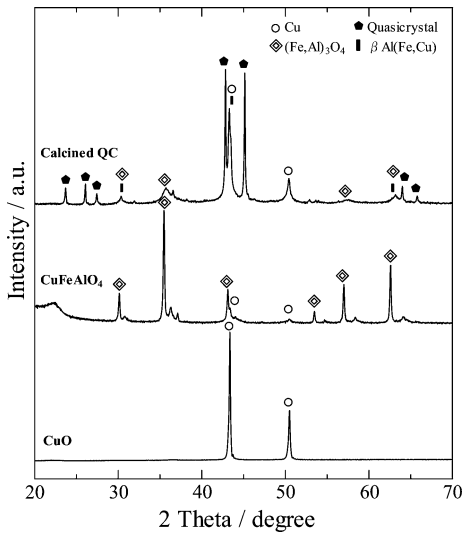

Fig. 8 Powder X-ray diffraction patterns for NaOH-leached Al–Cu–Fe QC alloy with calcination at 600 °C followed by H_2 reduction at 300 °C. Those for $CuFeAlO_4$ and CuO powder after reduction were shown for comparison

metallic Cu and $(Fe,Al)_3O_4$. These indicate that the $Cu_xFe_{3-x-y}Al_yO_4$ spinel on the *calcined QC* was reduced to metallic Cu and $(Fe,Al)_3O_4$ after H_2 reduction, in addition to the reduction of CuO to metallic Cu.

Figure 9a shows the bright field image of the *calcined QC* after H_2 reduction at 300 °C. Large metallic Cu particles (>100 nm) were clearly observed on the spinel layer of the reduced particle. Figure 9b is a dark-field image formed by the 2–20 reflection of metallic Cu. The bright contrast in the image corresponds to metallic Cu. It should be noted that very fine Cu particles (ca. 10 nm) were dispersed in the spinel layer, which are supposed to be account for high catalytic activity. The fine Cu particles in the spinel layer are generated from the reduction of $Cu_xFe_{3-x-y}Al_yO_4$. This can be inferred from that which the diffraction peaks of Cu were much broadening when the precursor was $CuFeAlO_4$ in the XRD patterns (Fig. 8). Whereas, large Cu particles on the spinel layer are generated from the reduction of CuO.

Active species of calcined QC for SRM reaction

Table 2 summarizes the physical properties and catalytic activities for SRM of leached QC alloy with and without calcination and those of related catalysts are also shown for comparison. Although mean crystallite size of Cu was large for the *calcined QC*, that of Cu particles observed in the spinel layer (Fig. 9b) was as small as those of Cu/ZnO and $CuFeAlO_4$. As above mentioned, CuO and $Cu_xFe_{3-x-y}Al_yO_4$ spinel were formed on the *calcined QC*. Among the related samples, CuO powder showed the lowest activities and $CuFeAlO_4$ spinel showed the highest activities in terms of H_2 production rate per surface area and per N_2O titration. Moreover, the activities of *calcined QC* were comparable to those of $CuFeAlO_4$ spinel. This indicates that the fine Cu particles generated from $CuFeAlO_4$ spinel showed higher level activity for SRM reaction. It is confirmed that the active species for SRM of the *calcined QC* is the fine Cu particles generated from $Cu_xFe_{3-x-y}Al_yO_4$ spinel after H_2 reduction. The formation of $Cu_xFe_{3-x-y}Al_yO_4$ spinel is a key factor for the enhancement of catalytic activity of the *calcined QC*. The CO selectivity of the catalysts except for CuO (under detection limit due to low activity) was the same level in this condition.

Recently, Cu-containing spinel (e.g., CuM_2O_4 type spinel) showing high performance in SRM [25], DME reforming [26], water gas shift reaction [27], and CO oxidation [28] have been reported. In previous reports, it has been commonly indicated that the active sites responsible for reactions are highly dispersed Cu species generated from Cu-containing spinel. However, the origin of high catalytic activity for the dispersed Cu species was not clear. The $Cu_xFe_{3-x-y}Al_yO_4$ spinel formed at the *calcined QC* is a good sample to understand this origin. Figure 10a is a SAD pattern taken from the spinel layer in Fig. 9, being assigned to [013] incidence of $(Fe,Al)_3O_4$. Apart from the diffraction spots responsible for $(Fe,Al)_3O_4$

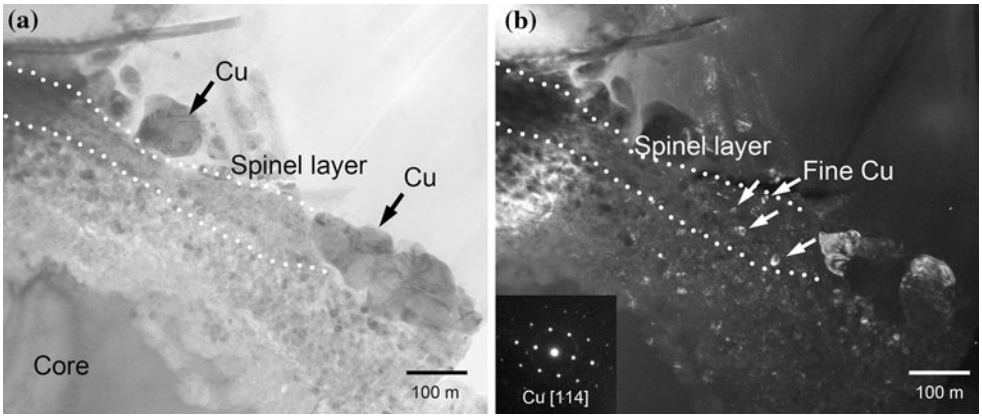

Fig. 9 **a** Bright field image of leached area of NaOH-leached Al–Cu–Fe QC alloy with calcination at 600 °C followed by H_2 reduction at 300 °C, **b** dark-field image using 2–20 reflection of Cu

Table 2 Physical properties and catalytic activities for SRM of NaOH-leached Al–Cu–Fe QC alloy with and without calcination at 600 °C and those of related catalysts for comparison

Catalyst	Cu crystallite size[b] (nm)	BET surface area (m^2/g_{-cat})	N_2O titration[d] ($\mu mol/g_{-cat}$)	H_2 production rate[e]			CO selectivity[e] (%)
				per catalyst weight ($\mu mol/s/g_{-cat}$)	per surface area ($\mu mol/s/m^2_{cat}$)	per N_2O titration ($\mu mol/s/\mu mol(N_2O)$)	
Leached QC	21	20.0	116.8	306.9	15.3	2.63	1.3
Leached QC with calcination	31 (10)[c]	5.0	126.6	405.0	81.0	3.20	1.2
Cu/ZnO[a]	10	57.3	262.2	372.2	6.5	1.42	1.5
CuO	66	2.4	12.2	15.4	6.4	1.26	–
$CuFeAlO_4$	13	1.7	67.7	242.2	142.4	3.58	1.2

[a] Prepared by coprecipitation method (Cu:Zn = 3:7 mol ratio)

[b] The crystallite size was obtained for Cu (200) peak of XRD of fresh samples (after reduction with 50% H_2/N_2 at 300 °C for 20 min) by Scherrer equation

[c] The crystallite size of fine Cu particles in the spinel layer (Fig. 9b) observed with TEM

[d] Total amount of N_2O consumption at 90 °C

[e] Reaction temperature at 300 °C

matrix, a number of spots due to metallic Cu were also clearly identified as shown in Fig. 10b which is also containing [013] incidence of Cu. There is one orientation relationship between $(Fe,Al)_3O_4$ matrix and Cu particles where Cu [013]//$(Fe,Al)_3O_4$ [013] and Cu (200)// $(Fe,Al)_3O_4$ (400), and thus the fine Cu particles took the same direction as $(Fe,Al)_3O_4$ matrix. This orientation relationship could be described as the illustration shown in Fig. 10c, which was observed very often in the $(Fe,Al)_3O_4$ spinel layers in the sample. Since both Cu and $(Fe,Al)_3O_4$ spinel are FCC structure, this orientation relationship are acceptable. This unique relationship indicates that the fine Cu particles generated from $Cu_xFe_{3-x-y}Al_yO_4$ interact with $(Fe,Al)_3O_4$ spinel matrix. This interaction of Cu with spinel matrix may stabilize active Cu nanoparticles against sintering upon catalytic reaction and it gives rise to high catalytic activity for SRM. In our previous paper [29], we have observed the same orientation relationship of Cu to Fe_3O_4 in reduced tetragonal $CuFe_2O_4$ spinel. The $CuFe_2O_4$ reduced by H_2 showed a self-assembled microstructure that exhibited fine dispersion of Cu within the porous Fe_3O_4 matrix and high catalytic activity and stability for SRM. Eguchi et al. [30] have reported that lattice matching at the interface between Cu and Fe_3O_4 in reduced $CuFe_2O_4$ and they have proposed a strong chemical interaction at the interface. From these reports and our results, we propose that one of the active sites of spinel structures in Cu-Fe–Al–O system is Cu species generated from the reduction of a spinel where Cu are oriented along the same direction with Fe_3O_4 (or $(Fe,Al)_3O_4$) matrix. One of the proposed configuration of several layers of Cu {111} on the {111} surface of Fe_3O_4 (or $(Fe,Al)_3O_4$) in reduced $CuFe_2O_4$ (or $Cu_xFe_{3-x-y}Al_yO_4$) spinel where Cu are oriented along the same direction with Fe_3O_4 (or $(Fe,Al)_3O_4$) is illustrated in

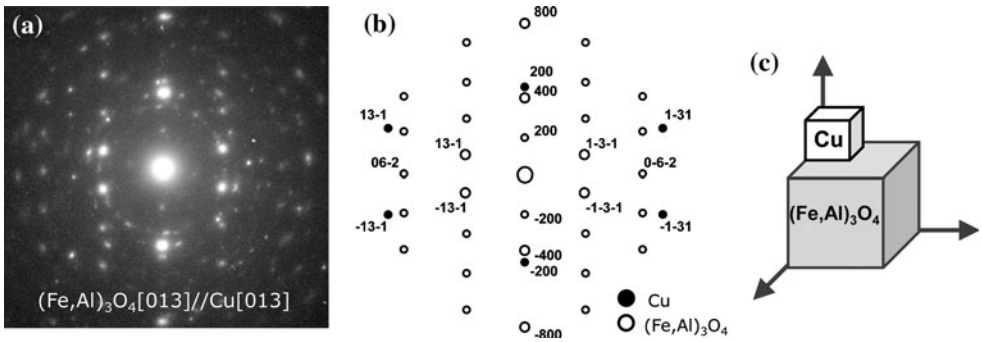

Fig. 10 **a** Selected area diffraction (SAD) pattern obtained from the spinel layer in Fig. 9a, **b** indexing of the pattern, and **c** illustration describing the orientation relationship between Cu and $(Fe,Al)_3O_4$

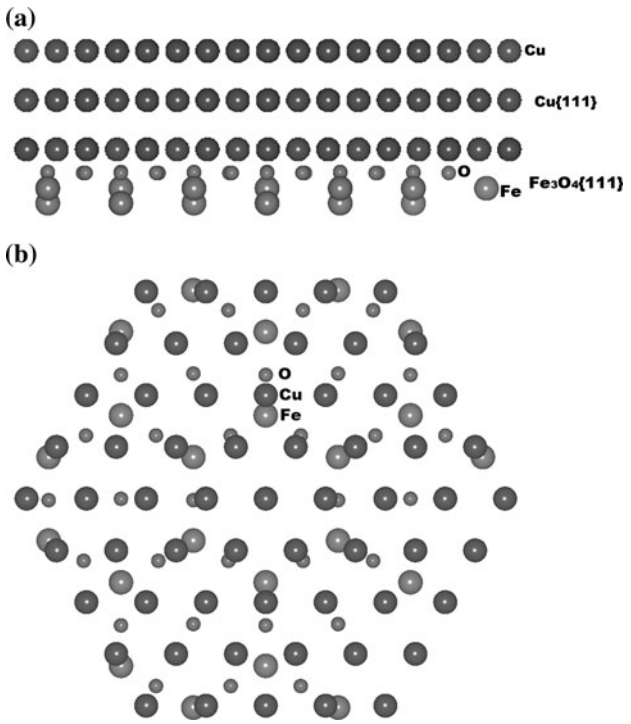

Fig. 11 Proposed configuration of several layers of Cu {111} on the {111} surface of Fe_3O_4 in reduced $CuFe_2O_4$ spinel, where Cu are oriented along the same direction with Fe_3O_4; **a** side view and **b** top view

Fig. 11. A strong Cu–O–Fe bonding may be expected in this configuration because of the proximity of Cu to O atoms in line and high symmetry. We anticipate that an orientation relationship of Cu and matrix will be observed in other Cu-containing spinel (e.g., $CuAl_2O_4$) and it would be the major contribution to those catalytic activities and stabilities.

In general, Cu-containing spinel phases are prepared by calcinations at high temperatures (e.g., above 900 °C for $CuFe_2O_4$). However, the present study reveals that $Cu_xFe_{3-x-y}Al_yO_4$ spinel is readily formed on the surface of leached QC alloy with calcination at 600 °C. Homogeneous mixture of oxides containing Cu, Fe, and Al in the leached layer of leached QC alloy would be easy to form $Cu_xFe_{3-x-y}Al_yO_4$ spinel with calcination at lower temperatures. This is an advantage of QC alloy while used as a precursor for catalyst.

This study could be simply understood as follows. The Al–Cu–Fe QC provided an environment for the formation of $Cu_xFe_{3-x-y}Al_yO_4$ spinel through leaching and consequent calcinations, and the resultant $Cu_xFe_{3-x-y}Al_yO_4$ spinel was a good precursor for generating active Cu nanoparticles those accounted for high catalytic activity.

Conclusions

We have studied evolution of microstructure of NaOH-leached Al–Cu–Fe QC alloy upon calcinations in air and its effects on catalytic activity. Conclusions are summarized in the following.

(1) A drastic increase in catalytic activity by about five times for SRM reaction over the NaOH-leached Al–Cu–Fe QC alloy was induced by calcinations in air at 600 °C.

(2) Cross-sectional observation with TEM revealed that the formation of the cubic $Cu_xFe_{3-x-y}Al_yO_4$ spinel structure at outermost layers of the leached QC alloy was induced by calcinations.

(3) All the samples were subjected to activation in H_2 at 300 °C prior to catalytic reaction. Upon this pre-treatment, the spinel structure decomposed to a composite structure with fine Cu nanoparticles dispersed in $(Fe,Al)_3O_4$ matrix, which gave rise to high activity. Drastic increase in catalytic activity is responsible for the fine Cu nanoparticles in the composite through the formation of $Cu_xFe_{3-x-y}Al_yO_4$ spinel structure.

(4) There is an orientation coincidence between the Cu nanoparticles and the $(Fe,Al)_3O_4$ matrix, where Cu are oriented along the same direction with the matrix, e.g., Cu [013]//$(Fe,Al)_3O_4$ [013] and Cu (200)//$(Fe,Al)_3O_4$ (400). This orientation relationship may stabilize the Cu nanoparticles through a bonding of Cu–O–Fe, against sintering of Cu upon catalytic reaction.

Acknowledgements The authors thank Dr. D. Morikawa at Tohoku University for his valuable comments and suggestions and thank Prof. M. Terauchi at Tohoku University for his support. The synchrotron radiation experiments were performed at the BL15XU in SPring-8 with a help of Dr. Y. Matsushita and Dr. M. Tanaka (NIMS) and approval of the Japan Synchrotron Radiation Research Institute (JASRI). This work was supported by Global COE Program "Materials Integration, Tohoku University," Ministry of education, culture, sports, science and technology (MEXT)-Japan.

References

1. Shechtman D, Blech I, Gratias D, Cahn JW (1984) Phys Rev Lett 53:1951
2. Tsai AP (1990) In: Stadnik ZM (ed) Physical properties of quasicrystals. Springer, Berlin, p 5
3. Kajiwara K, Suzuki S, Sato H, Hata K (2009) Z Kristallogr 224:5
4. Hao J, Cheng H, Wang H, Cai S, Zhao F (2007) J Mol Catal A 271:42
5. Tsai AP, Yoshimura M (2001) Appl Catal A 214:237
6. Yoshimura M, Tsai AP (2002) J Alloys Compd 342:451
7. Kameoka S, Tanabe T, Tsai AP (2004) Catal Today 93–95:23
8. Tanabe T, Kameoka S, Tsai AP (2006) Catal Today 111:153
9. Ngoc BP, Geantet C, Aouine M, Bergeret G, Raffy S, Marlin S (2008) Int J Hydrogen Energy 33:1000
10. Highfield J, Liu T, Loo YS, Grushko B, Borgna A (2009) Phys Chem Chem Phys 11:1196
11. Ngoc BP, Geantet C, Dalmon JA, Aouine M, Bergeret G, Delichere P, Raffy S, Marlin S (2009) Catal Lett 131:59
12. Raney M (1927) US Patent 1 628 190
13. Smith AJ, Munroe PR, Tran T, Wainwright MS (2001) J Mater Sci 36:3519. doi:10.1023/A:1017984618032
14. Tanabe T, Kameoka S, Sato F, Terauchi M, Tsai AP (2007) Philos Mag 87:3103
15. Tanabe T, Kameoka S, Tsai AP (2010) Appl Cat A 384:241
16. Evans JW, Wainwright MS, Bridgewater AJ, Young DJ (1983) Appl Catal 7:75
17. Gines MJL, Amadeo N, Laborde M, Apesteguia CR (1995) Appl Catal A 131:283
18. Saito M, Tomoda K, Takahara I, Murata K, Inaba M (2003) Catal Lett 89:11
19. Tsai AP, Inoue A, Masumoto T (1987) Jpn J Appl Phys 26:1505
20. Tsvigunov AN, Apolenis AV, Annikov VE, Raikova VM (2007) Glass Ceram 64:429
21. Lee SH, Chae KP, Lee YB, Oh KS (1990) Solid State Commun 74:1
22. Shannon RD, Prewitt CT (1969) Acta Crystallogr B 25:925
23. Vanderstraten PJM, Metselaar R (1980) J Appl Phys 51:3236
24. Shimoda N, Faungnawakij K, Kikuchi R, Fukunaga T, Eguchi K (2009) Appl Catal A 365:71
25. Kameoka S, Tanabe T, Tsai AP (2005) Catal Lett 100:89
26. Tanaka Y, Kikuchi R, Takeguchi T, Eguchi K (2005) Appl Catal B 57:211
27. Tanaka Y, Utaka T, Kikuchi R, Takeguchi T, Sasaki K, Eguchi K (2003) J Catal 215:271
28. Severino F, Brito JL, Laine J, Fierro JLG, Agudo AL (1998) J Catal 177:82
29. Kameoka S, Tanabe T, Tsai AP (2010) Appl Catal A 375:163
30. Eguchi K, Shimoda N, Faungnawakij K, Matsui T, Kikuchi R, Kawashima S (2008) Appl Catal B 80:156
31. Oneill HS, Dollase WA (1994) Phys Chem Miner 20:541
32. Nickel EH (1973) Can Miner 11:1003
33. Hill RJ (1984) Am Miner 69:937